BRACELET BUS-NA 98 BZ 67 - BRONZE - IRON AGE - SWITZERLAND

Artefact name Bracelet bus-na 98 BZ 67

Authors Naima. Gutknecht (HE-Arc CR, Neuchâtel, Neuchâtel, Switzerland) & Valentina. Valbi (Laboratoire Métallurgie et Culture LMC-IRAMAT-CNRS-UTBM, Belfort, Franche-Comté, France)

Url /artefacts/1010/

The object



Credit Service archéologique de l'Etat de Fribourg, M-J.Scholl.

Fig. 1: Two fragments of a bracelet from Bussy/Pré de Fond (Switzerland),

Description and visual observation

Description of the artefact Fragments of a bracelet with curvature (Fig. 1); internal surface of the curvature with a central rib and hammer marks; external surface of the curvature with decorative incisions; round section.

Type of artefact Jewellery

Origin Bussy/Pré de Fond, Fribourg, Fribourg, Switzerland

Recovering date 1998

Chronology category Iron Age

chronology tpq 550 B.C.

chronology taq 450 B.C.

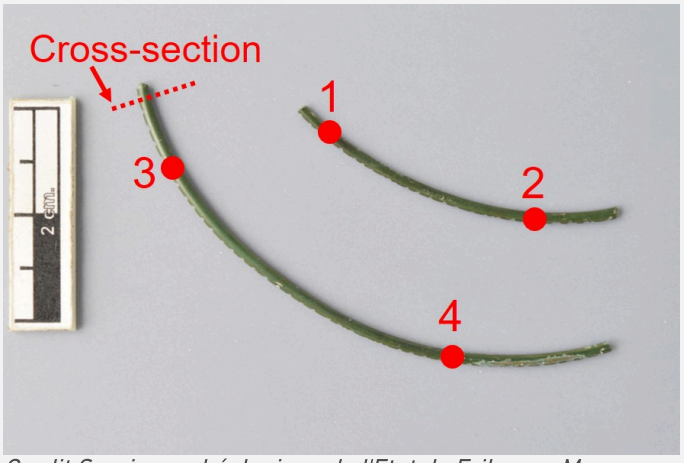
This work is licensed under CC BY-NC-ND 4.0

Chronology comment	First Iron Age - Hallstatt Culture (Ha D2-3)
Burial conditions / environment	Soil
Artefact location	Archaeological Service of the Fribourg Canton, Fribourg
Owner	Archaeological Service of the Fribourg Canton, Fribourg
Inv. number	bus-na 98 BZ 67
Recorded conservation data	Mechanical cleaning of the external corrosion products and soils

Complementary information

This bracelet is part of a corpus of four bracelets (***bracelets bus-na 98 BZ 11 / bus-na 98 BZ 23 / bus-na 98 BZ 38 / bus-na 98 BZ 67***) found on the same site.

Study area(s)



Credit Service archéologique de l'Etat de Fribourg, M-J.Scholl/HE-Arc CR, N.Gutknecht.

Fig. 2: Two fragments of a bracelet showing the sampling area and the XRF analysis areas (red dots),

Binocular observation and representation of the corrosion structure

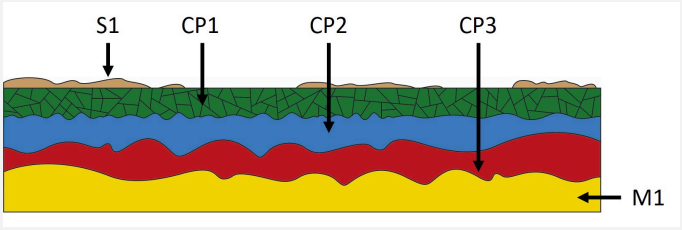
The schematic representation below gives an overview of the corrosion structure encountered on the bracelet from a first visual macroscopic observation.

Strata	Type of stratum	Principal characteristics
S1	Soil	light yellow, thin, non-compact, powdery
CP1	Corroded product	dark green, thick, discontinuous, compact, hard, network cracks
CP2	Corroded product	dark blue, thin, discontinuous, non-compact, very soft
CP3	Corroded product	dark red, thin, continuous, compact, soft
M1	Metal	yellow, metallic, compact, soft

Table 1: Description of the principal characteristics of the strata as observed under binocular and described according to Bertholon's method.

The transition between CP3 and the metal M1 is irregular. CP1 shows a network of cracks on the whole stratum.

This work is licensed under CC BY-NC-ND 4.0



Credit HE-Arc CR, N.Gutknecht.

Fig.3: Stratigraphic representation of the corrosion structure of the bracelet by macroscopic and binocular observation,

MiCorr stratigraphy(ies) – Bi

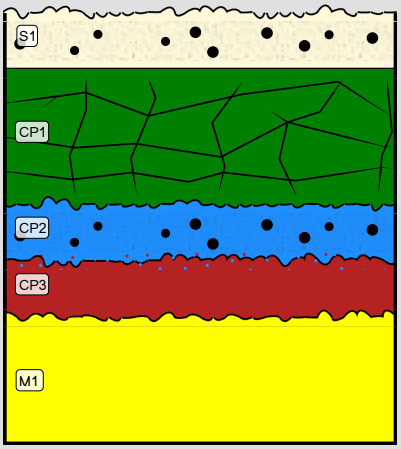
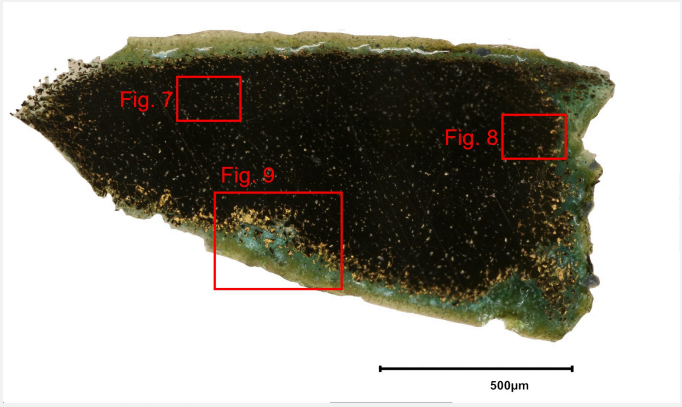


Fig. 4: Stratigraphic representation of the corrosion structure of the bracelet observed macroscopically under binocular microscope using the MiCorr application with reference to the whole Fig. 3. The characteristics of the strata are only accessible by clicking on the drawing that redirects you to the search tool by stratigraphy representation, Credit HE-Arc CR, N.Gutknecht.

Sample(s)



Credit LMC-CNRS, V.Valbi.

Fig. 5: Micrograph of the cross-section of the sample taken from the bracelet (Fig. 2) in dark field showing the location of Figs. 7 to 9,

Description of sample	The cross-section corresponds to a lateral cut (Fig. 2) and is representative of the entire thickness of the bracelet's body. A metallic core is present below the corrosion layers (Fig. 6)
Alloy	Bronze
Technology	Cold worked with repeated annealing and final cold working
Lab number of sample	ébauche 67
Sample location	Archaeological Service of the Fribourg Canton, Fribourg

This work is licensed under CC BY-NC-ND 4.0

Responsible institution	Archaeological Service of the Fribourg Canton, Fribourg
Date and aim of sampling	February 2020. Metallographic study.

Complementary information

None.

Analyses and results

Analyses performed:

Non-invasive approach

- XRF with handheld portable X-ray fluorescence spectrometer (NITON XL3t 950 Air GOLDD+, Thermo Fischer®). General Metal mode, acquisition time 60s (filters: Li20/Lo20/M20).

Invasive approach (on the sample)

- Optical microscopy: the sample is polished, then it is observed on a numerical microscope KEYENCE VHX-7000 in bright and dark field.
- Metallography: the polished sample is etched with alcoholic ferric chloride and observed by optical microscopy in bright field.
- SEM-EDS: the sample is coated with a carbon layer and analyses are performed on a SEM-FEG JEOL 7001-F equipped with a silicon-drift EDS Oxford detector (Aztec analysis software) with an accelerating voltage of 20 kV and probe current at about 9 nA. The relative error is considered of about 10% for content range <1mass%, and of 2% for content range of >1mass%.
- µ-Raman spectroscopy: it is performed on a HORIBA Labram Xplora spectrometer equipped of a 532 nm laser with 1800 grating, the laser power employed is between 0.04 and 0.55 mW with acquisition time varying between 1 and 5 minutes.

Non invasive analysis

The XRF analysis of the bracelet was carried out before sampling on four areas on the two fragments (Fig. 2). All strata (soil, corrosion products, and metal) are analyzed at the same time. The metal is presumably a copper-tin alloy with some lead, while the other elements detected (Si, Al) are from the burial environment.

Elements (mass %)	1	2	3	4
Cu	45	44	46	50
Sn	36	36	34	30
Pb	7	7	9	9
Si	8	8	9	9
Al	>2	53	3	3

Table 2: Chemical composition of the surface of the bracelet at four representative points shown in Fig.2. Method of analysis: XRF. The results are rounded up to the nearest whole number.

Metal

EDX analysis (Table 3) of the residual metal on cross-section indicates that it is a high tin bronze (14 mass% Sn) with a high percentage of Pb (4 mass%).

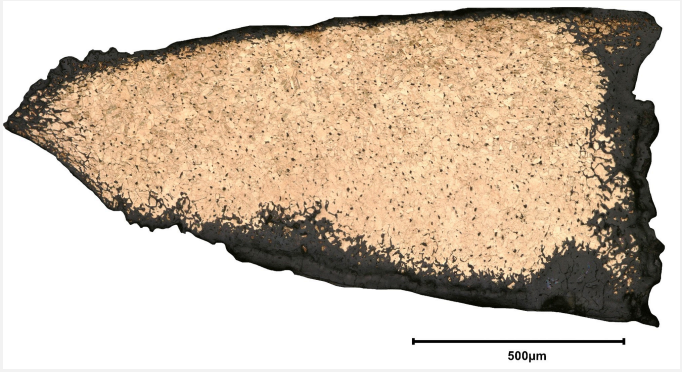
The metal has a grain structure (Fig. 7) with several twinned grains (Figs. 7 and 8), indicating that the object underwent an annealing procedure. On the whole sample, it is possible to observe the presence of slip lines (Figs. 7

This work is licensed under CC BY-NC-ND 4.0

and 8) caused by cold mechanical working of the metal after annealing. Numerous lead inclusions (Figs. 7 and 10) of dimension of around 10 µm are homogeneously distributed on the whole surface of the sample. Intergranular corrosion is observed (Figs. 6 and 8).

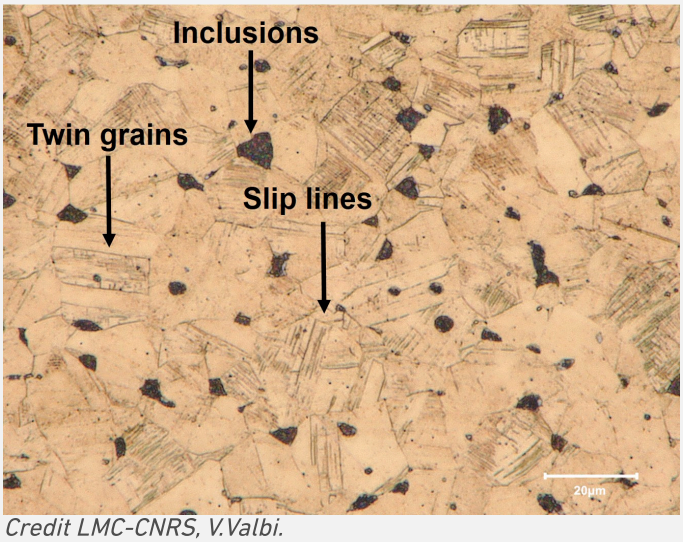
Elements	mass %
Cu	81
Sn	13.9
Pb	4.0
As	<0.5
Ni	<0.5
Si	<0.5

Table 3: Chemical composition of the alloy over a general area of analysis obtained by SEM-EDX.



Credit LMC-CNRS, V.Valbi.

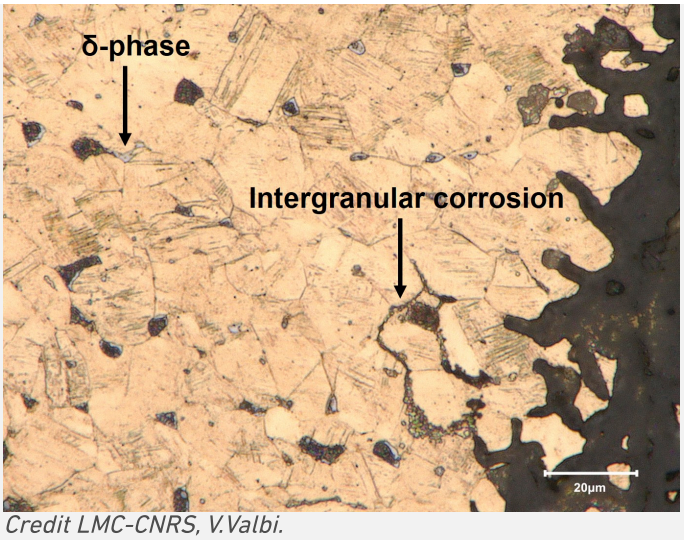
Fig. 6: Micrograph of the etched cross-section of the sample taken from the bracelet (Fig. 2) in bright field,



Credit LMC-CNRS, V.Valbi.

Fig. 7: Micrograph of the metal sample from Fig. 5 (detail), etched, bright field. Elongated grains with slip lines are observed, as well as grey lead inclusions,

This work is licensed under CC BY-NC-ND 4.0



Credit LMC-CNRS, V.Valbi.

Fig.8: Micrograph of the metal sample from Fig. 5 (detail), etched, bright field. Equiaxed grains with slip lines are observed, as well as black lead inclusions and grey eutectic phase,

Microstructure	Polygonal grains with inclusions
First metal element	Cu
Other metal elements	Sn, Pb

Complementary information

The interface roughness between the metal and the CPs, corresponding to the stratum identified as corroded metal (CM1), was measured through optical microscopy observation and the following parameters were determined (in µm): Rp=96, Rv = 25, Rt = 121, Ra = 35.

Corrosion layers

The observation of the sample in cross section in dark field (Figs. 5 and 9) allowed to identify an external continuous light green stratum (CP1), a dark green stratum (CP2) and a corroded metal stratum (CM1).

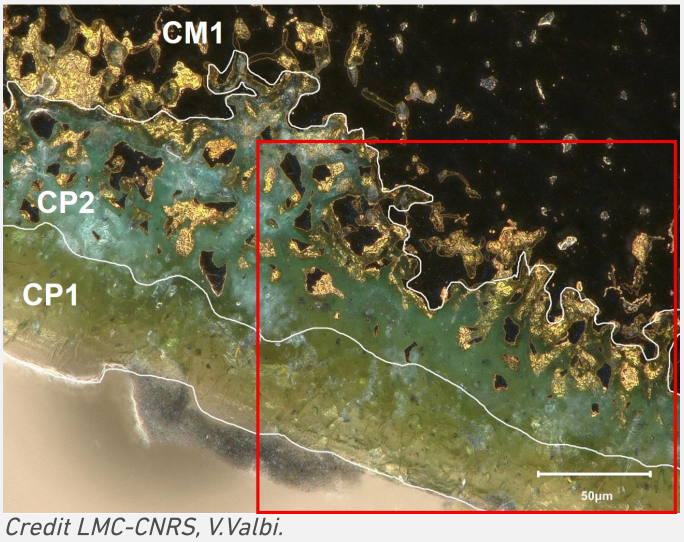
The EDX elemental analysis (Table 4) and mapping (Fig. 10) of the visually identified CPs by binocular and cross-sectional observations show that CP1 is Cu depleted, O and Sn enriched and polluted with Ca, Si and P from the soil, while CP2 is also Cu depleted and O and Sn rich but with less external polluting elements. These results are in agreement with the preliminary XRF analysis that already showed an enrichment in O and Sn and a depletion in Cu from the surface. No enrichment in Pb was though observed in cross-section.

	CP1	CP2
Cu	10.4	18.9
Sn	45.6	46.6
O	32.5	26.2
Pb	3.8	4.2
Si	3.5	2.6
Ca	2.0	1.0
P	1.0	0.6
Cr	<0.5	n.d.
Fe	<0.5	n.d.
Ni	<0.5	n.d.
Al	< 0.5	n.d.

Table 4: Chemical composition (mass%) of the corrosion layers over a general area of analysis in cross-section obtained by SEM-EDX.

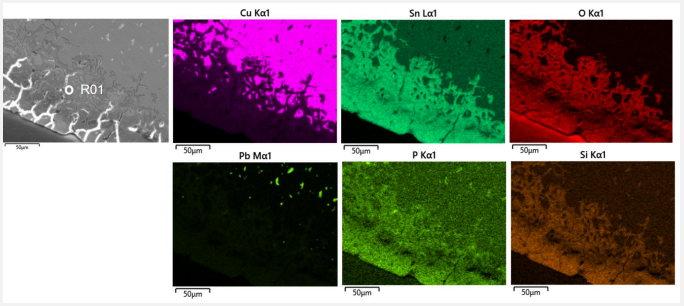
This work is licensed under CC BY-NC-ND 4.0

Analyses with μ-Raman were performed on the identified strata. The R01 (Fig. 11) point of analysis was performed on the green CP2 layer and the obtained spectrum has a broad peak at 560 cm^{-1} that can be attributed to nanocrystals of cassiterite Sn_2O thanks to comparison with the work of Ospitali et al. 2012. The analysis point performed on the green external CP1 was too disturbed by fluorescence signal and an identification of the phase was impossible.



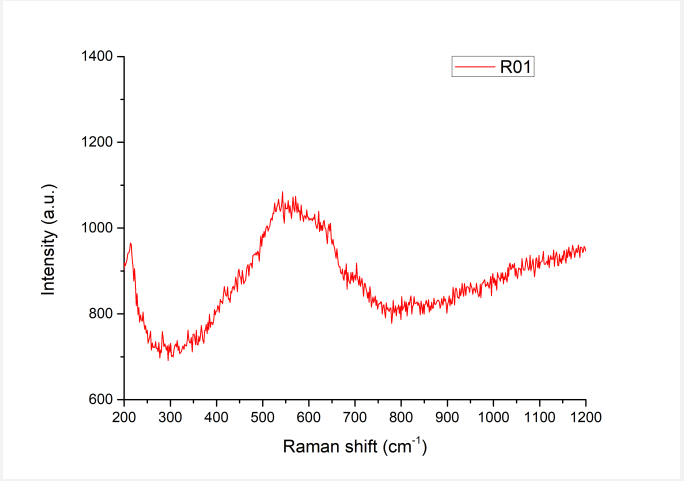
Credit LMC-CNRS, V.Valbi.

Fig. 9: Micrography of the corrosion structure from Fig. 5 (detail): light green CP1 and green CP2. The SEM-EDX analysis area from Fig. 10 is indicated by the red rectangle,



Credit LMC-CNRS, V.Valbi.

Fig. 10: SEM image, BSE-mode, and elemental chemical distribution of the selected area. The selected point for Raman analysis shown in Fig. 11 is indicated,



Credit LMC-CNRS, V.Valbi.

Fig. 11: Raman spectrum of the analysis point in Fig. 10, identified as nanocassiterite according to Ospitali et al. 2012,

Corrosion form	Uniform
Corrosion type	Type I (Robbiola)

Complementary information

None.

This work is licensed under CC BY-NC-ND 4.0

MiCorr stratigraphy(ies) – CS

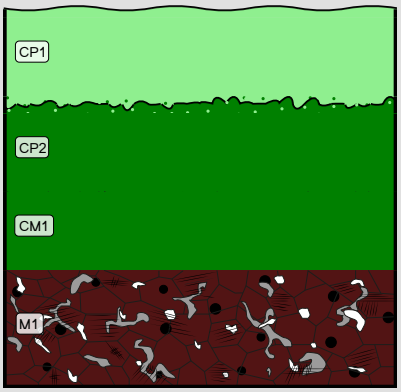


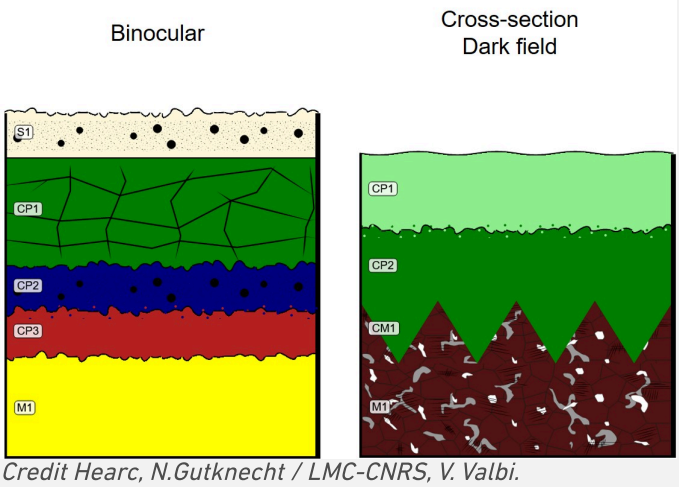
Fig. 12: Stratigraphic representation of the sample observed in cross-section under dark field using the MiCorr application. The characteristics of the strata are only accessible by clicking on the drawing that redirects you to the search tool by stratigraphy representation. This representation was build according to Fig. 9, Credit LMC-CNRS, V.Valbi.

Synthesis of the binocular / cross-section examination of the corrosion structure

One S and three CPs were identified by binocular observation, while two CPs and a CM were observed in cross-section.

The CP1 and CP2 observed in binocular observation correspond to the CP1 and CP2 observed in cross-section. The internal CP3 layer identified by binocular observation was not observed in cross-section. This could be explained by a discontinuous CP3 strata on the object.

The outer sediment layer (S1), easily identified under binocular, was not visible in the cross-section. On the contrary, the presence of a CM1 stratum was only revealed through cross-section observation. Moreover, information obtained under binocular examination such as brightness, compactness, cohesion, and adherence are not accessible during cross-sectional observation. Conversely, the physico-chemical characteristics obtained by cross-section examination are not easily accessible during the binocular examination. The differences observed underline the necessity and complementarity of these two approaches.



Credit Hearc, N.Gutknecht / LMC-CNRS, V. Valbi.

Fig. 13: Stratigraphic representation side by side of binocular view and cross-section (dark field),

Conclusion

The bracelet is a tin bronze with Pb inclusions. The metallographic observation revealed that the metal was cold-worked, annealed, and has received final cold-working, in agreement with the surface decoration observed on the object.

This work is licensed under CC BY-NC-ND 4.0

The characterization of the corrosion products showed a typical corrosion structure for an archeological bronze. The object presents the phenomenon of decuprification with Sn enrichment. This is a common phenomenon observed on bronze archaeological objects buried in moderately aggressive natural conditions (such as oxygenated sandy soils). The enrichment in Ca, P and Si in the CP1 was also previously observed on archaeological objects (Robbiola et al. 1998, Papadopoulou et al. 2016) and can be attributed to the diffusion of these elements from the burial soil.

The good conservation condition of the original surface located, according to the Bertholon's method, at the interface of CP1 with S1 allows to identify the corrosion form as a Type I (according to Robbiola et al. 1998 classification). CP1 presents hammering traces and decoration which are typical markers of the original surface.

This bracelet is part of a corpus of four bracelets (***bracelets bus-na 98 BZ 11 / bus-na 98 BZ 23 / bus-na 98 BZ 38 / bus-na 98 BZ 67***) found on the same site. These artefacts are all drafts of bracelets but correspond to different stages of advancement: two bracelets are "as cast" and present no further working (***bracelet bus-na 98 BZ 23*** and ***bus-na 98 BZ 38***) while two bracelets present signs of annealing and cold-working (***bracelet bus-na 98 BZ 11*** and ***bus-na 98 BZ 67***).

References

References on object and sample

1. MiCorr_Bracelet bus-na 98 BZ 11
2. MiCorr_Bracelet bus-na 98 BZ 23
3. MiCorr_Bracelet bus-na 98 BZ 38

References on analytical methods and interpretation

4. Bertholon, R. (2001) Characterization and location of the original surface of corroded archaeological objects. Surface Engineering, 17 (3), 241-245.
5. Degrigny, C., Gaspoz, C., Rosselet, A., Boissonnas, V., Jeanneret, R. and Bertholon, R. (2016) The MIFAC-Metal Online project: developing a Decision Support System for locally invasive diagnosis of heritage metals, in METAL 2016, proceedings of the ICOM-CC Metal WG interim meeting, eds. R. Menon, C. Chemello and A. Pandya, New Dehli, (India), 220-227.
6. Lafuente, B., Downs, R. T., Yang, H., Stone, N. (2015) The power of databases: the RRUFF project. In: Highlights in Mineralogical Crystallography, T. Armbruster and R. M. Danisi, eds. Berlin, Germany, W. De Gruyter, 1-30.
7. Ospitali, F., Chiavari, C., Martini, C., Bernardi, E., Passarini, F., Robbiola, L. (2012) The characterization of Sn-based corrosion products in ancient bronzes: a Raman approach. Journal of Raman Spectrpscopy, 43 (11), 1596-1603.
8. Papadopoulou, O., Vassiliou, P., Grassini, S., Angelini, E. and Gouda, V. (2016) Soil-induced corrosion of ancient Roman brass – A case study. Materials and Corrosion, 67, No. 2.
9. Scott, D. (2006) Metallography and microstructure of ancient and historic metals. J Paul Getty Museum Publications.
10. Robbiola L., Blengino M., Fiaud C., (1998) Morphology and mechanisms of formation of natural patinas on archaeological Cu–Sn alloys. Corrosion Science, 40 (12), 2083-2111.

This work is licensed under CC BY-NC-ND 4.0